A microreactor array for spatially resolved measurement of catalytic activity for high-throughput catalysis science

Petro Kondratyuk [a,b], Gamze Gumuslu [b], Shantanu Shukla [b], James B. Miller [a,b], Bryan D. Morreale [a], Andrew J. Gellman [a,b,*]

[a] National Energy Technology Laboratory, Pittsburgh, PA 15236, United States
[b] Dept. of Chemical Engineering, Carnegie Mellon University, Pittsburgh, PA 15213, United States

ARTICLE INFO

ABSTRACT

We describe a 100-channel microreactor array capable of spatially resolved measurement of catalytic activity across the surface of a flat substrate. When used in conjunction with a composition spread alloy film (CSAF, e.g., $Pd_xCu_yAu_{1-x-y}$) across which component concentrations vary smoothly, such measurements permit high-throughput analysis of catalytic activity and selectivity as a function of catalyst composition. In the reported implementation, the system achieves spatial resolution of 1 mm^2 over a 10×10 mm^2 area. During operation, the reactant gases are delivered at constant flow rate to 100 points of differing composition on the CSAF surface by means of a 100-channel microfluidic device. After coming into contact with the CSAF catalyst surface, the product gas mixture from each of the 100 points is withdrawn separately through a set of 100 isolated channels for analysis using a mass spectrometer. We demonstrate the operation of the device on a $Pd_xCu_yAu_{1-x-y}$ CSAF catalyzing the H_2-D_2 exchange reaction at 333 K. In essentially a single experiment, we measured the catalytic activity over a broad swathe of concentrations from the ternary composition space of the $Pd_xCu_yAu_{1-x-y}$ alloy.

© 2013 Elsevier Inc. All rights reserved.

1. Introduction

The advantages of high-throughput synthesis, characterization, and analysis of materials have been understood since as early as 1955 when a composition library was used in the determination of the Ag–Pb–Sn phase diagram [1]. Several years later, rapid phase mapping was demonstrated on a co-deposited Fe–Cr–Ni composition spread alloy film [2]. Nevertheless, the real growth and popularization of high-throughput methods occurred with the advent of automated data acquisition and computational data analysis. Starting in the 1990s, such methods were used for purposes ranging from the detection of a photoluminescent compound in the Gd–Ga–O system [3] to mapping the magnetic properties of Tb–Co–Ni–Fe alloys [4,5].

One of the most widely used sample preparation methods for high-throughput materials science is the deposition of several different compositions side by side on a flat substrate, followed by automated, spatially resolved characterization of the resulting composition library. We adopt this approach to deposit metal alloy films in which the composition varies smoothly as a function of position on the substrate (Fig. 1). Hereafter, such films will be

referred to as composition spread alloy films (CSAFs). In principle, a CSAF on a flat substrate can contain all compositions of a binary (e.g., Pd–Cu) or a ternary (e.g., Pd–Cu–Au) alloy.

A number of techniques have been used to prepare composition libraries. In one group of methods, the components are initially deposited as different layers using binary masks or moving edge masks [6–8]. A moving edge mask results in the deposition of a film whose thickness varies across the surface. In the case of binary masks, a rectangular array of cells with different compositions is produced. This approach, however, suffers from its reliance on solid-state diffusion to achieve component mixing within the film, as it is deposited in a layer-by-layer fashion. Another group of methods uses co-deposition from several sources operating simultaneously to produce a mixed film [9]. Frequently, no mask is employed during the deposition, and the concentration of the component is determined by the distance from the source in question [10–12]. In this case, the sources are usually positioned off-axis with respect to the substrate center. Shadow masks and slit masks can also be used, if a different concentration profile is desired [13–15].

In this work, $Pd_xCu_yAu_{1-x-y}$ CSAFs were prepared using an offset-filament evaporative source, described in detail elsewhere [16]. The source relies on three simultaneously operating, linear evaporative elements that are positioned around the substrate with an offset relative to its center. The concentration gradient

---

* Corresponding author at: Dept. of Chemical Engineering, Carnegie Mellon University, Pittsburgh, PA 15213, United States. Fax: +1 412 268 3848.
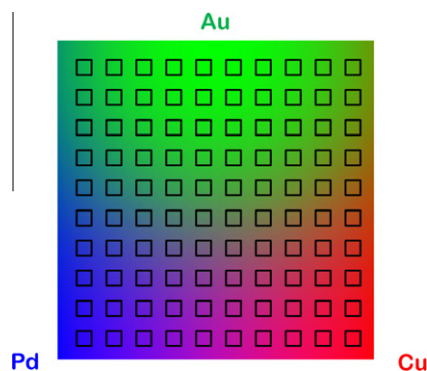E-mail address: gellman@cmu.edu (A.J. Gellman).

Fig. 1. Schematic illustration of a $Pd_xCu_yAu_{1-x-y}$ CSAF with the analysis regions of the catalytic microreactor array marked as squares arranged in a 10×10 grid. The array covers an area of 10 mm × 10 mm and the microreactor regions have dimensions of 900 μm × 700 μm.

results from the fact that each point on the substrate surface has a different set of distances from the three filament sources.

High-throughput techniques are a natural methodology for catalysis researchers, given the very large number of materials and process variables that affect the performance of catalysts. It is, therefore, not surprising that high-throughput characterization of catalysts has been a very active area of research (see, for example [17–19], and the references therein). A majority of publications focus on parallelizing the preparation and characterization of many discrete samples; [20] is a good example for this approach.

High-throughput methods employing composition libraries and CSAFs in particular have the potential to contribute significantly to catalysis science and to catalyst discovery and evaluation. However, probing the catalytic activity of isolated points across a flat CSAF surface presents an experimental challenge, namely the reactants need to be delivered to a specified region on the CSAF surface and the product gases extracted from that region in such a way that the gas streams to and from adjacent regions on the surface are isolated from one another. One way to accomplish this is to use a scanning probe incorporating a flow channel for gas delivery and withdrawal from a specific point underneath the probe as it moves over the sample surface. Scanning probe systems have been described previously [21–23]. However, because in this configuration the history of exposure of the sample to the reactants varies from point to point across the sample surface, scanning probe systems are difficult to implement for materials that display activity changes over time (i.e., activation or deactivation). Ideally, one needs to have all points across the CSAF catalyst library subject to the same history and running in a catalytic steady state for extended periods of time.

In the work presented here, a multichannel microreactor array has been developed that allows 100 parallel gas streams to contact 100 different points (alloy compositions) on a 1 cm² CSAF surface. The reactions at each point on the CSAF can reach steady state, and all 100 microreactors are running continuously and in parallel. The gases are delivered to and from the catalytic surface through a glass microfluidic device that directs the flow to 100 analysis points arranged in a 10×10 grid across the CSAF surface. The microfluidic device defines a square array of microreactors bounded on one side by the CSAF catalyst surface and isolated from one another by a gasket. Because the gas is continually fed to all analysis points, this approach enables high-throughput measurements as a function of time to be performed relatively easily and under well-controlled flow conditions. The ability to measure catalyst activity as a function of time allows studies of catalyst evolution during reaction, something that cannot be easily studied in a

high-throughput mode by using a scanning probe. Similarly, the gas mixture flowing through the reactors and the temperature can be varied to collect kinetic data from all points across the CSAF surface in parallel.

Two techniques are combined in this work to allow high-throughput measurement of the catalytic activity of an alloy film as a function of elemental composition: deposition of a CSAF followed by spatially resolved measurement of its catalytic activity with a microreactor array. The CSAF deposition tool is described elsewhere [16]. The principal goal of this paper is to discuss the design, construction, and operation of the microreactor array.

2. Experimental

2.1. Design and fabrication of the microreactor array

The core component of the apparatus for high-throughput study of catalytic reactivity is a multichannel microreactor array that continuously delivers reactant gases to 100 isolated regions on a CSAF surface and withdraws the products from each region for mass spectrometric analysis. The analysis regions have dimensions of 900 μm × 700 μm and are arranged in a 10×10 square array with a center-to-center spacing of 1 mm. Fig. 1 illustrates the CSAF surface with three components in red, green, and blue with a 10×10 grid of squares which represent the 100 regions isolated for analysis.

The construction of the multichannel microreactor array is shown schematically in Fig. 2. It consists of 22 glass layers, each layer having a pattern of micromachined channels for gas flow. Thin, flat borosilicate glass sheets (Shott Borofloat®, 36 mm × 27 mm × 700 μm thick) were used as the starting material for the layers. In order to achieve the necessary density of channels at the sample surface, the thickness of the glass sheets was reduced to 500 μm by polishing prior to micromachining the gas flow channels onto one side of each sheet. The channels are roughly rectangular in cross-section, measuring 500 μm wide and 200–250 μm deep. The cross-sectional area and shape of the channels do not influence the flow rate through the channel, because the channels provide much less resistance to gas flow than the glass capillaries connected to them to deliver and extract the gases.

There are two types of glass layers in the microreactor device that differ in their channel patterns (Fig. 2a). Ten of the layers are used for the delivery of reactant gas to the CSAF surface; they split the single inlet stream for the layer into 10 parallel reactant channels. The other 10 layers route the product gas streams away from the CSAF surface to the gas analysis system. Each of these product gas layers has 10 parallel channels running from one end of the microarray device to the other. The 10 reactant channel layers and 10 product channel layers are stacked alternately (Fig. 2b) and solid glass cover plates are added at the two sides of the device. This channel arrangement allows the gas to be delivered to each of 100 regions on the CSAF film (Fig. 1a) and withdrawn through separate, isolated pathways.

To fabricate the solid glass microreactor array, the 22 glass layers were bonded together using a procedure that was developed to produce reliable bonding between many layers. The process does not use any bonding agents; it relies on the fact that flat, clean glass plates can bond to one another after appropriate chemical treatment, for example soaking in concentrated sulfuric acid [24]. We found that in the case of borosilicate glass, treatment with 20% aqueous NaOH solution for 2 h gives even better results than treatment in H_2SO_4. After soaking in NaOH solution, the layers are washed under a flow of deionized water and, while still wet, stacked in the correct order and left for 24 h to allow the water to evaporate. At the end of this drying step, the layers are already
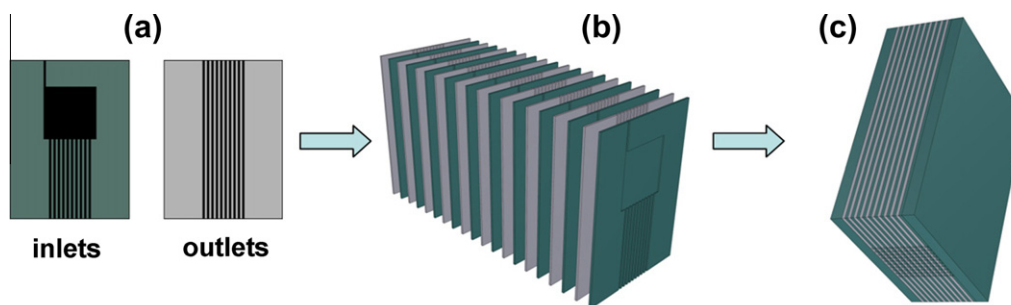
Fig. 2. The design of the 100-channel microreactor array used to deliver and withdraw gases from the CSAF surface. (a) Input and output channels are machined into flat glass sheets. (b) 10 input and 10 output layers are interleaved and bonded together with cover plates. (c) The side of the microfluidic device having 100 inputs and 100 outputs is ground and polished. This side of the device is mated with a gasket having 100 holes which is then sandwiched between the glass reactor and the CSAF catalyst surface.

bonded to one another, although not very tightly. The remainder of the water is evaporated in a vacuum oven (2 h at room temperature, 2 h at 90 °C, and 3 h at 180 °C), after which the microfluidic device is placed into a furnace and annealed for 1 h at 620 °C. At this temperature, the glass becomes soft enough for permanent bonds to form between the layers, but not soft enough for the channel structure or the shape of the device to be adversely affected. After this annealing step, the glass layers are tightly bonded to one another and form a solid block. Although some bonding defects are always present and can be observed as interference fringes, they usually occur at the edges of the glass sheets and do not impact the channel structure.

After bonding, the side of the array having 100 reactant gas inlets and 100 product gas outlets (Fig. 2c) is polished to a high degree of flatness, with typical deviations from flatness of less than 250 nm. Ultimately, this polished side of the device will be mated via a gasket with the CSAF surface. Each input–output pair on the reactor array side delivers and extracts gasses from one region on the CSAF surface. As will be described in more detail below, a flexible gasket with a 10×10 array of holes is needed to isolate each input–output pair from its neighbors. Gases flow to and from the microreactor array through 360 µm ID polyimide-coated quartz capillaries (Polymicro Technologies, Inc.). The capillaries are glued into the channel holes on the back side of the glass microreactor block with a silicone sealant capable of withstanding temperatures up to 250 °C. Reactant gases flow from a gas manifold through a single capillary tube to a 1-to-10 flow splitter. This divides the reactant gas stream into 10 capillaries that carry the gas mixture into the microreactor block (one capillary per input layer). Within each input layer, the flow is further divided into 10 channels that go to the feed inlets of the 100 microreactors. At the end of the inlet channels, the reactant gases come into contact with the CSAF catalyst surface at 100 regions of different composition isolated from one another by the 100 holes in the gasket. The gases flow over the heated CSAF surface to the outlet channels. The product gasses flow through the channels of the outlet plates into 100 isolated capillaries leading from the microreactor block to the sampling and analysis system.

The capillary connections to the microreactor channels are the points of highest (and dominant) resistance to flow in the gas flow path. Therefore, the lengths of the capillaries connecting to the microreactor block need to be identical to guarantee that the flow rates through different channels are equal.

2.2. Reactant gas delivery

The required mixture of reactant gases is delivered to the microfluidic device using mass flow controllers (Aalborg Instruments, GFC-17). Ideally, the reaction in the microreactor array should progress far enough so that the product concentration is easily measurable, but at the same time should not come too close to equilibrium or to 100% conversion. At equilibrium, the differences in catalytic activity across the CSAF cannot be detected. In other words, to make useful kinetic comparisons of catalytic activity, the reactors need to operate in the differential conversion regime. Given that the area of the catalyst surface in each reaction channel is quite small (on the order of 0.6 mm²), low flow rates through the channels increase microreactor residence times and consequently allow for higher conversion, which is useful for relatively inactive catalysts. Conversely, if the activity is high, higher flow rates may be necessary to prevent the reaction from approaching equilibrium.

An additional consideration puts a lower limit on the allowable flow rates: the structure of the microfluidic device is such that at low rates, product gases may diffuse back up the inlet channels against the flow of reactant gas and then mix with the inlet streams of neighboring channels. This undesirable cross-talk is eliminated by keeping the flow above a certain threshold. In the catalytic activity measurements described below, the total gas flow rate was 30 ml/min (or 0.30 ml/min per channel), which was sufficiently high to prevent back-diffusion.

Flow rates through individual channels were also measured experimentally by switching the gas flow from Ar to N_2 at the microreactor array input and measuring the times for N_2 to reach the end of the output capillary for each channel. We found that the standard deviation of the travel times for the 100 channels was 3.6% of their mean value. Given that travel times and conductance through the channel are inversely related, this number also characterizes the standard deviation in the flow rates through individual channels.

2.3. Product gas sampling and analysis

The product gas streams from each of the 100 microreactors are analyzed using a quadrupole mass spectrometer (Stanford Research Systems RGA-200). In order to select which channel, and thereby which region of the CSAF surface, is analyzed at any given time by the mass spectrometer, an automated 100-channel sampler was designed and constructed (Fig. 3). A quartz capillary with an internal diameter of 10 µm is connected directly to the vacuum chamber housing the mass spectrometer and serves as the sampling capillary. The other end of the sampling capillary is mounted to an x–y positioning stage. Its two orthogonal linear motion stages, each driven by a programmable stepper motor, insert the sampling capillary into the gas streams from 100 output capillaries carrying product gas from the multichannel microreactor array. To guide the end of the sampling capillary, tapered steel funnels are connected to the ends of each of the 100 output capillaries.
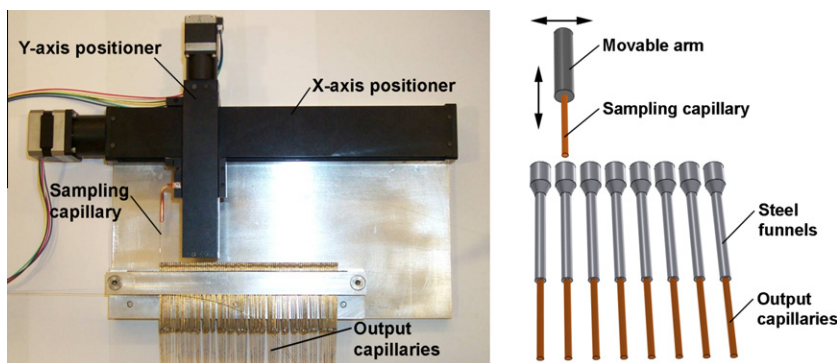
Fig. 3. Photograph of the programmable, multichannel sampler (left) and a schematic demonstrating its operation (right). The sampler selects the output channel from which the gas will be sampled for analysis by the mass spectrometer. It consists of two orthogonal linear positioning stages that translate a single 10 μm internal diameter sampling capillary, inserting it into the gas stream from one of 100 output channels.

At low volumetric flow rates through the channels, diffusion of air against the product gas flow may occur at the open sampling end of the output capillaries. Not surprisingly, the diffusion of air is most pronounced in the case of light product gases (for example, H_2, HD, or D_2). Similar difficulties with air diffusion against the flow of products were observed by Claus et al. [25], who constructed a conceptually similar sampling device. This can be minimized by increasing the total flow rate.

The microreactor sampler can be programmed to select gasses from the microreactors in any order and for selected sampling times. In a typical experiment, sampling from a single channel takes approximately 7 s. This time is spent moving the sampling capillary to a new channel, waiting for the product gas to reach the mass spectrometer and taking signal readings at several q/m ratios. The total time for the analysis of gases from all 100 channels is, therefore, ~12 min.

2.4. Gasket for the isolation of reaction channels

To achieve the desired spatial resolution of catalytic activity across the CSAF, the gas flow coming into contact with each compositionally distinct region on the CSAF surface must be isolated from the gas flows contacting neighboring regions. Undesired intermixing can occur easily at the interface of the microreactor array and the CSAF catalyst surface. In the current implementation of the microreactor array, neighboring regions are isolated from one another by means of an elastomer gasket that has 100 precisely positioned, rectangular holes (700 μm × 900 μm) cut through it using a laser (Fig. 4). Each hole in the gasket encircles a single feed-effluent channel pair on the polished surface of the microreactor array. During the measurements of catalytic reactivity, the gasket is compressed between the microreactor and the CSAF

Fig. 4. (Left) Optical image of the polished front face of the microreactor array showing inlet and outlet channel openings. (Right) A laser-machined elastomer gasket used to isolate each inlet–outlet pair from its neighbors. The rectangular windows in the gasket define 100 reaction areas (700 μm × 900 μm) on the CSAF.

sample under study. The effectiveness of the gasket for the elimination of intermixing of gases between neighboring reaction channels is illustrated in Fig. 5. These measurements were taken using a 10-channel microreactor array in which different gases could be fed into the different reaction channels. In this particular experiment, the gas feed in channel 5 was pure Ar, while pure N_2 was fed through the remaining nine channels. Each pair of feed-effluent holes on the microfluidic device was connected with a groove through which the gases could pass even when no gasket was present. The effluent gasses in each of the channels were monitored with the mass spectrometer. In the absence of a gasket (Fig. 5, right panel), the Ar gas from channel 5 is detected in neighboring channels and a significant amount of N_2 is detected in channel 5. This intermixing is observed in spite of the fact that both the reactor face of the microreactor array and the counterfacing sample surface were polished to a high degree of flatness (with a deviation of less than 250 nm). It appears that this intermixing is a result of the unavoidable presence of dust particles trapped between the two surfaces and creating a gap between them. When a gasket made out of perfluorinated elastomer (Viton) is used to isolate the feed-effluent pairs of each of the 10 microreactors in the array, there is no detectable mixing of gases between channels. The left panel of Fig. 5 shows the results of an experiment with the 10-channel array in which pure Ar was fed into channel 5 and pure N_2 into the other nine channels. In this experiment, a gasket with 10 holes isolating each feed-effluent pair was positioned between the reactor face and the counter face and as a result, both Ar and N_2 stay in their respective channels.

Gaskets made from several materials including Kapton, silicone rubber, Viton, Kalrez, and graphite were tested with the microreactor array. Perfluoroelastomer Kalrez 7075 (Dupont) was found to be the most suitable material. Highly elastic rubbers (Viton, silicone rubber) were very effective in preventing intermixing but were easily distorted during compression and heating, to the point of blocking gas flow channels. Harder materials, such as Kapton and graphite, retained their shape well under pressure and were stable at temperatures over 550 K, but were not soft enough to provide gas-tight seals. Kalrez gaskets, on the other hand, did not distort at temperatures up to 590 K and provided excellent inter-channel isolation.

2.5. Sensitivity limits of detectable catalytic turnover frequency

The most useful metric of the sensitivity of the microreactor array is the minimum detectable turnover frequency (*TOF*) as this will dictate the types of catalytic reactions that are amenable to study. The limiting factor in this case is the detection limit of the
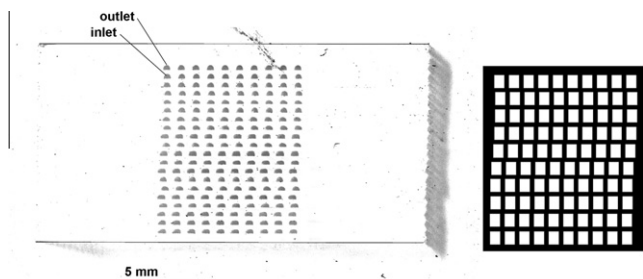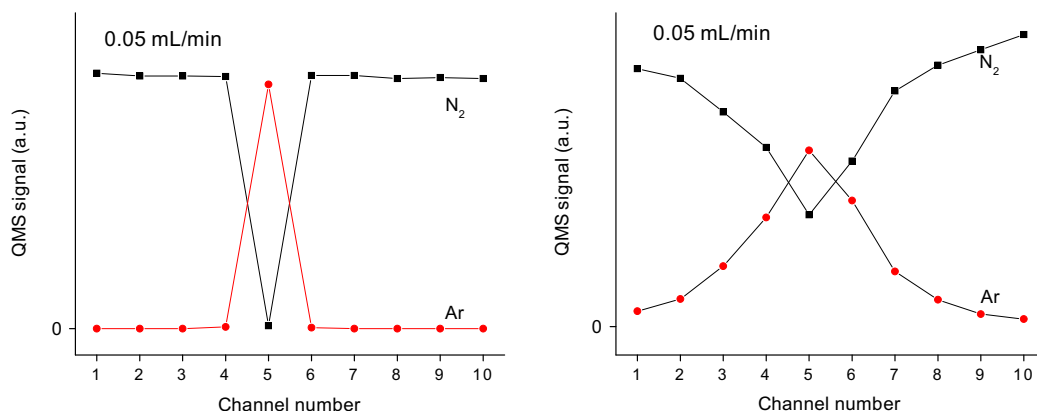
Fig. 5. The effectiveness of the elastomer gasket for preventing intermixing of gases between adjacent channels of the microreactor array. Left: With a Viton gasket, Ar (in channel 5) and N_2 (in the rest of the channels) remain separated after the gases pass through the microreactor array. Right: Without a gasket, pure Ar fed into channel 5 diffuses into the other channels, which are fed with pure N_2.

mass spectrometer. The SRS-RGA-200 used in this work is equipped with an electron multiplier giving it a published detection limit of $S = 10^{-7}$, which is fairly standard for simple residual gas analyzers (RGA) with electron multipliers. Higher sensitivity quadrupole mass spectrometers can achieve $S = 10^{-11}$. At atmospheric pressure, the reactant gas flow rate through each microreactor is $F = 0.30$ ml/min $= 10^{17}$ molec/s. Under these conditions, the minimum detectable product yield with a high sensitivity mass spectrometer is $Y_{min} = S \cdot F = 10^6$ molec/s. Given a catalyst area of $A = 10^{-2}$ cm^2, the number of catalyst atoms or catalytic sites per reactor is $N = 10^{13}$. Thus, the minimum detectable catalytic activity with a high sensitivity quadrupole mass spectrometer would be $TOF_{min} = 10^{-7}$ molec/site/s. Realistically, the use of the microreactor array for a study of catalytic reaction kinetics that span a few orders of magnitude across temperature or catalysts composition would require a reaction with a $TOF = 10^{-4}$ at the highest temperature (600 K) or on the highest activity alloy. With the standard RGA used in this work, this viable detection limit is $TOF = 1$. Note that the catalytic conversion at these minimum detection limits is 10^{-5}, well within the differential conversion range. The sensitivity of the microreactor array coupled with a mass spectrometer as the detector is sufficiently high that it will allow study of a wide variety of catalytic processes including olefin hydrogenation, acetylene hydrogenation, and partial oxidation reactions [26–29].

3. Measurements of catalytic activity in Pd$_x$Cu$_y$Au$_{1-x-y}$ alloys

3.1. H$_2$–D$_2$ exchange and hydrogen purification membranes

In order to test the operation of the microreactor array, several Pd$_x$Cu$_y$Au$_{1-x-y}$ CSAFs were prepared and the microreactor array was used to measure their catalytic activity for the H$_2$–D$_2$ exchange reaction. H$_2$–D$_2$ exchange occurs readily on transition metals such as Pt, Pd, or Ni which dissociatively adsorb H$_2$. Either the dissociative molecular H$_2$ adsorption or associative H atom desorption steps can be rate-limiting depending on the catalyst [30]. This reaction is interesting from the industrial point of view because it is directly relevant to the processes that occur on Pd-based H$_2$ separation membranes. In order to pass through such a membrane, H$_2$ must dissociatively adsorb on the membrane surface, diffuse through the metal in the form of H atoms, and associatively desorb from the other side [31–33]. H$_2$–D$_2$ exchange experiments probe the kinetics of two of these three stages, the dissociative adsorption and associative desorption. Therefore, reactivity in the H$_2$–D$_2$ exchange is an important factor in determining the suitability of Pd alloys for H$_2$ separation membranes.

Pure Pd suffers from two significant drawbacks when used in hydrogen purification membranes. It tends to have poor mechanical stability when exposed to H$_2$ due to hydride formation, and it is easily poisoned by H$_2$S, a common minor component in coal-derived gas streams [34–36]. In order to address these weaknesses, it is alloyed with other metals such as Cu, Ag, and Au [36–41]; the performance of these alloys in H$_2$–D$_2$ exchange can be characterized in a straightforward way with the microreactor array.

If the H$_2$–D$_2$ exchange reaction is allowed to reach completion, an equilibrium mixture of H$_2$, D$_2$, and HD is produced. When starting from an equimolar mixture of H$_2$ and D$_2$, the equilibrium ratios of H$_2$:D$_2$:HD are close to the "random permutation" concentrations of 0.25:0.25:0.5, with a slight temperature-dependent deviation due to isotope effects. The exact ratios can be found from the expression for the equilibrium constant [42].

$$\frac{P_{HD}^2}{P_{H_2} \cdot P_{D_2}} = 4.16 \cdot \exp\left[-\frac{77.7K}{T}\right] \tag{1}$$

This equation gives the equilibrium HD fraction of 0.472 at 300 K, 0.480 at 400 K, and 0.485 at 500 K. In our catalytic reactivity measurements, the flow rates of reactants were held sufficiently high (30 mL/min total flow) that they prevented the product concentrations from approaching the equilibrium values. Experimentally, the concentrations following the reaction on the catalytic CSAF were
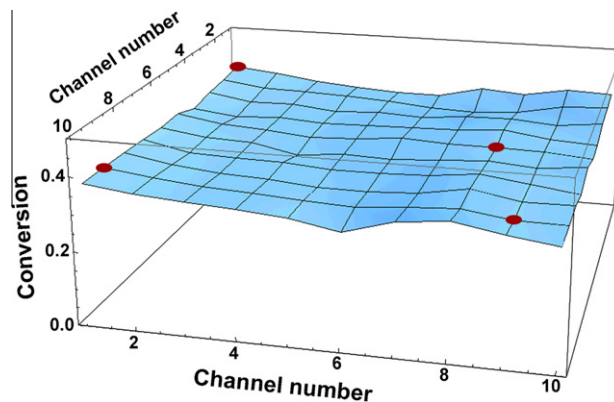

Fig. 6. Conversion in the H$_2$–D$_2$ reaction at 433 K over a pure Pd film as measured by the microreactor array. Equilibrium conversion is 0.48. Uniform activity is observed with a mean conversion of 0.34 ± 0.015. Four blocked reaction channels are marked with red circles; the conversion values at these locations were substituted with the averages calculated from the adjacent channels. Flow rates of H$_2$ and D$_2$ were 15 mL/min for each gas.

determined by measuring the mass spectrometer signals at $m/q = 2$ (H_2), 3 (HD), and 4 (D_2) amu.

3.2. H_2–D_2 exchange on Pd and on $Pd_xCu_yAu_{1-x-y}$

The conversion in the H_2–D_2 exchange reaction measured with the microreactor array over a Pd-only film at 433 K is shown in Fig. 6. The film was deposited by evaporation onto a polished, polycrystalline Mo substrate at room temperature under UHV conditions. X-ray photoemission spectroscopy (XPS) measurements at several locations on the film did not detect Mo, indicating that the film thickness was greater than 10 nm. After deposition, the Mo substrate with the Pd film was transferred in air onto the microreactor array, and an equimolar mixture of H_2 and D_2 was passed through the 100 reaction channels. A flexible Kalrez gasket was used between the CSAF surface and the microreactor array to ensure isolation of neighboring reaction channels from one another. As expected, a relatively uniform reactivity profile across the 10 mm × 10 mm surface was measured by the microreactor array, with a mean conversion of 0.34 ± 0.015. The equilibrium conversion at this temperature is 0.48. Four channels of the microreactor array did not function during the experiment because of blockage in the inlet capillaries; these channels are marked with red circles in Fig. 6. The conversion values at these locations could not be measured and are replaced in the figure with the averages calculated from the neighboring channels.

Notably, we found that the reactivity of Pd-based catalytic CSAFs for H_2–D_2 exchange decreased significantly after annealing the films in vacuum at 700–800 K. This effect was seen for pure Pd films as well as Pd_xCu_{1-x} and $Pd_xCu_yAu_{1-x-y}$ alloys. For example, the conversion over an annealed pure Pd film at 433 K was ~0.10, compared to the conversion of 0.34 measured on the as-prepared Pd film shown in Fig. 6. It appears likely that the decrease in reactivity resulting from annealing was due to the crystallization of CSAFs. Electron backscatter diffraction (EBSD) tests indicated that the as-prepared films were largely amorphous (they displayed no clear diffraction pattern), whereas the annealed films showed clear diffraction from the expected bulk crystal lattice. The amorphous nature of the as-deposited CSAF could provide favorable H_2 adsorption sites that are missing on the annealed (crystalline) films.

The $Pd_xCu_yAu_{1-x-y}$ CSAFs were also deposited onto polycrystalline Mo substrates using an offset-filament evaporative tool [16]. Separate evaporation sources for Pd, Cu, and Au were used. The deposition rate of each metal was controlled by choosing the temperature of its evaporator. All three metals were deposited simultaneously until the film was approximately 80 nm thick in the center of the substrate.

After deposition, the $Pd_xCu_yAu_{1-x-y}$ CSAFs were characterized by spatially resolved X-ray photoemission spectroscopy (Thermo Fisher Thetaprobe) to determine the elemental composition across a 10 mm × 10 mm area of the substrate. A composition map for the three components of a $Pd_xCu_yAu_{1-x-y}$ CSAF is shown in Fig. 7; the location of the greatest concentration for each element was determined by the orientation of the evaporation sources during the film deposition. The size of the X-ray spot on the CSAF during these measurements was approximately 200 μm × 400 μm. This CSAF covers a range of compositions in the Cu-rich side of the ternary diagram.

To conduct H_2–D_2 exchange over the $Pd_xCu_yAu_{1-x-y}$ CSAF, the substrate was heated resistively to 333 K and an equimolar mixture of H_2 and D_2 was flowed through the microreactor array at a total rate of 30 mL/min (0.3 mL/min per channel). The map of HD concentration in the product gas following the reaction on the surface is shown in Fig. 8 on the left. Using the XPS elemental compositions from Fig. 7, the activity can be plotted on the Pd–Cu–Au ternary diagram (Fig. 8, right).

Several observations may be made with regard to the composition dependence of the catalytic reactivity in this ternary $Pd_xCu_yAu_{1-x-y}$ alloy. The reactivity is clearly nonlinear in Pd concentration; a large region rich in Cu and Au is completely inactive, despite the presence of Pd in the alloy. At these reaction temperatures, H_2–D_2 exchange only begins when Cu atomic fraction falls below ~65%. As the concentration of Cu drops even further, the reactivity appears to reach a plateau. It can also be noted that the iso-conversion contours in the ternary diagram are not parallel to the iso-Pd lines; in fact, they are more aligned with iso-Cu lines. This means that diluting Pd with Cu has a stronger inhibitory effect on reactivity than diluting with Au. The primary objective of Fig. 8, however, is to demonstrate clearly that the microchannel array is capable of resolving catalytic activity across a ternary alloy composition space.

3.3. High-throughput microreactor characteristics

As mentioned previously, there are a variety of strategies that have been developed for high-throughput catalysis [17–19]. There are a number of differentiating factors that can be used to compare them and no single strategy is optimal for the study of all types of catalytic processes or for addressing all catalyst performance characteristics. Some of the key differentiating factors are as follows: the strategy for the preparation of catalyst libraries; the range of catalyst materials compatible with the preparation methods; the capabilities for the characterization of those catalyst libraries; the range of operating conditions over which catalytic activity can be measured; and the sensitivity and specificity of the product detection scheme.

The preparation of CSAFs as catalyst libraries allows all compositions to be deposited simultaneously rather than sequentially
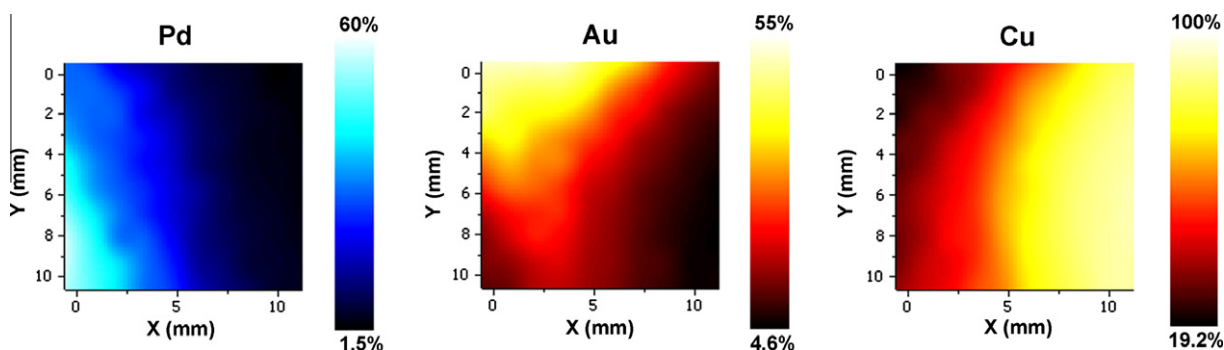
Fig. 7. Concentration distribution (at.%) obtained with XPS for Pd (left), Au (center), and Cu (right) in a $Pd_xCu_yAu_{1-x-y}$ CSAF. The measurement area is 10 mm × 10 mm and the XPS spot size was 200 μm × 400 μm.
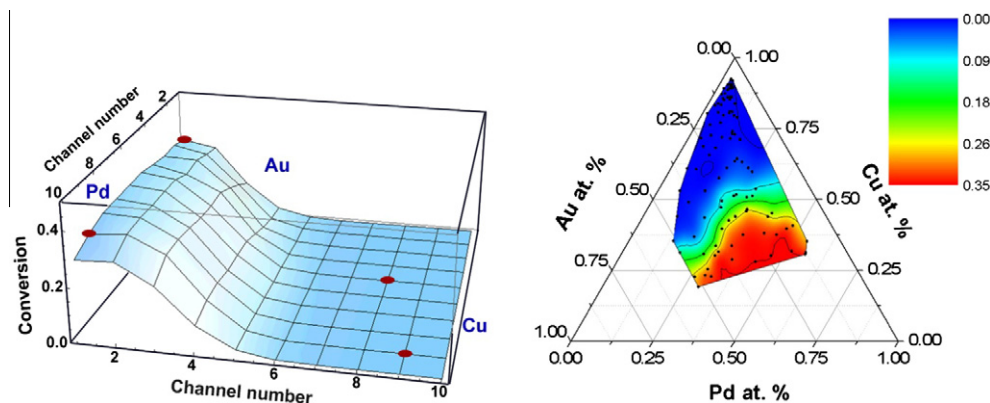
Fig. 8. (Left) Conversion in the H_2–D_2 reaction over the $Pd_xCu_yAu_{1-x-y}$ CSAF measured at 333 K. Reaction equilibrium at this temperature corresponds a conversion of 0.48. Four channels marked with red circles were blocked, and the conversion values at these locations were substituted with the averages from adjacent channels. (Right) Activity plotted as a function of composition on a ternary diagram. (For the interpretation of the references to color in this figure legend, the reader is referred to the web version of this article.)

and is fairly easy, given the right instrumentation [10,15,16]. The CSAF platform for catalyst libraries is also quite versatile in its scope for use with many multicomponent materials, but not infinitely so. For example, CSAFs can be prepared from most metals in the periodic table and they can be prepared in the form of non-metallic materials such as oxides, carbides, and nitrides. However, it is hard to imagine, although maybe not impossible, that catalytic materials such as zeolites or metal organic frameworks could be prepared in the form of CSAFs. Finally, the CSAFs have the virtue that they are readily characterized using a wide range of spatially resolved surface analysis tools such as XPS, Auger electron spectroscopy, and X-ray diffraction.

One of the key features of the high-throughput multichannel microreactor array described in this report is that it allows the study of catalytic activity in such a way that all 100 catalyst compositions have exactly the same reaction history. All are running in parallel with continuous exposure to the reactant stream. The limitations associated with its current design are its temperature range (300–600 K) and a pressure range up to 1 atm. Of course, the reactant pressures can be maintained at <1 atm provided that they are diluted in an inert gas to a total pressure of 1 atm. Although the current design is limited in these parameters, there is no reason, in principle, that one could not fabricate a high-throughput, multichannel microreactor array from steel with much the same design as ours and such that it could operate at higher pressures and higher temperatures.

Finally, the types of reactions that can be studied in the multichannel microreactor are determined by the fact that we have chosen to use mass spectrometry for product detection. As determined earlier, mass spectrometry is sufficiently sensitive that it will allow the study of a wide variety of reactions provided that their $TOF > 10^{-4}$ within the range of accessible temperatures and catalyst compositions. However, mass spectrometry is not appropriate for the analysis of the product streams of some catalytic processes. In our case, where conversion may be very low and sensitivity is an issue, mass spectrometry will work best when the product is heavier than the reactants, and therefore, there will be no overlap of the reactant fragmentation pattern with the product fragmentation pattern. Olefin hydrogenation or epoxidation reactions would be good examples. However, reactions with multiple products that are not easily distinguished using mass spectrometry would not be appropriate for study. For example, determining the product distribution of the Fischer–Tropsch reaction using mass spectrometry would be futile because the fragmentation patterns of the products overlap one another. Nonetheless, the multichannel microreactor array coupled with CSAFs will allow the fundamental study of many important catalytic processes across a wide range of alloy catalyst composition space.

4. Conclusions

We have presented a new methodology and instrumentation for high-throughput study of alloy catalysts. It is based on the deposition of composition spread alloy films (CSAFs), in which component concentrations vary across the substrate, followed by spatially resolved characterization of their catalytic properties with a 100-channel microreactor array. The microreactor array continually delivers reactant gases to 100 points on the CSAF surface, enabling time-resolved studies of changes in the catalytic activity, such as changes due to poisoning, activation, or sintering (in the case of particles). It is capable of mass spectrometric analysis of the gas effluents from the 100 channels with a time resolution of ~10 min, if all channels are sampled sequentially. In the current implementation, the operating temperature range is 300–600 K and the operating pressure is limited to 1 atm; however, feed stream dilution with an inert gas allows use of a wide range of reactant partial pressures.

We have demonstrated the functionality of the 100-channel microreactor by studying the catalytic activity of $Pd_xCu_yAu_{1-x-y}$ alloys for the H_2–D_2 exchange reaction. We found a nonlinear dependence of activity on Pd content, with no activity present in the Cu-rich region, and stronger inhibition of activity by dilution with Cu than with Au. These high-throughput catalysis techniques promise to be especially powerful when combined with spatially resolved surface analysis to correlate the reactivity at different alloy compositions with changes in other surface characteristics.

References

[1] A. Boettcher, G. Haase, R. Thun, Z. Metallkd. 46 (5) (1955) 386–400.
[2] K. Kennedy, T. Stefansky, G. Davy, V.F. Zackay, E.R. Parker, J. Appl. Phys. 36 (12) (1965) 3808–3810.
[3] J.S. Wang, Y. Yoo, C. Gao, I. Takeuchi, X.D. Sun, H.Y. Chang, X.D. Xiang, P.G. Schultz, Science 279 (5357) (1998) 1712–1714.
[4] S.E. Russek, W.E. Bailey, G. Alers, D.L. Abraham, IEEE Trans. Magn. 37 (4) (2001) 2156–2158.
[5] S.E. Russek, P. Kabos, R.D. McMichael, C.G. Lee, W.E. Bailey, R. Ewasko, S.C. Sanders, J. Appl. Phys. 91 (10) (2002) 8659–8661.
[6] Y.K. Yoo, F. Duewer, H.T. Yang, D. Yi, J.W. Li, X.D. Xiang, Nature 406 (6797) (2000) 704–708.
[7] X.D. Xiang, X.D. Sun, G. Briceno, Y.L. Lou, K.A. Wang, H.Y. Chang, W.G. Wallacefreedman, S.W. Chen, P.G. Schultz, Science 268 (5218) (1995) 1738–1740.
[8] K.W. Kim, M.K. Jeon, K.S. Oh, T.S. Kim, Y.S. Kim, S.I. Woo, Proc. Natl. Acad. Sci. USA 104 (4) (2007) 1134–1139.
[9] R.B. van Dover, L.F. Schneemeyer, Macromol. Rapid Commun. 25 (1) (2004) 150–157.
[10] S. Guerin, B.E. Hayden, C.E. Lee, C. Mormiche, A.E. Russell, J. Phys. Chem. B 110 (29) (2006) 14355–14362.
[11] Y. Yamada, T. Fukumura, M. Ikeda, M. Ohtani, H. Toyosaki, A. Ohtomo, F. Matsukura, H. Ohno, M. Kawasaki, J. Supercond. 18 (1) (2005) 109–113.
[12] R.C. Smith, I. Hoilien, J. Chien, S.A. Campbell, J.T. Roberts, W.L. Gladfelter, Chem. Mater. 15 (1) (2003) 292–298.
[13] R.F. Egerton, J.C. Bennett, J. Micros. – Oxford 183 (1996) 116–123.
[14] S. Guerin, B.E. Hayden, J. Comb. Chem. 8 (1) (2006) 66–73.
[15] B. Fleutot, J.B. Miller, A.J. Gellman, J. Vac. Sci. Technol. – A 30 (6) (2012) 061511.
[16] D. Priyadarshini, P. Kondratyuk, J.B. Miller, A.J. Gellman, J. Vac. Sci. Technol. – A 30 (2012) 011503.
[17] A. Hagemeyer, P. Strasser, A.F. Volpe, High-throughput Screening in Heterogeneous [i.e. chemical] Catalysis, Wiley-VCH, Weinheim, 2004. xx, 319 p. (Great Britain).
[18] D. Farrusseng, Surf. Sci. Rep. 63 (11) (2008) 487–513.
[19] S.I. Woo, S.H. Kim, Top. Catal. 53 (1–2) (2010) 1-1.
[20] S.M. Senkan, Nature 394 (6691) (1998) 350–353.
[21] P.J. Cong, A. Dehestani, R. Doolen, D.M. Giaquinta, S.H. Guan, V. Markov, D. Poojary, K. Self, H. Turner, W.H. Weinberg, Proc. Natl. Acad. Sci. USA 96 (20) (1999) 11077–11080.
[22] N. Li, K. Eckhard, J. Assmann, V. Hagen, H. Otto, X.X. Chen, W. Schuhmann, M. Muhler, Rev. Sci. Instrum. 77 (8) (2006).
[23] N. Li, J. Assmann, W. Schuhmann, M. Muhler, Anal. Chem. 79 (15) (2007) 5674–5681.
[24] Z.J. Jia, Q. Fang, Z.L. Fang, Anal. Chem. 76 (18) (2004) 5597–5602.
[25] P. Claus, D. Honicke, T. Zech, Catal. Today 67 (4) (2001) 319–339.
[26] M. Boudart, Chem. Rev. 95 (3) (1995) 661–666.
[27] H. Molero, D. Stacchiola, W.T. Tysoe, Catal. Lett. 101 (3–4) (2005) 145–149.
[28] D. Duca, F. Frusteri, A. Parmaliana, G. Deganello, Appl. Catal. A – Gen. 146 (2) (1996) 269–284.
[29] H.S. Wu, S.C. Chung, J. Comb. Chem. 9 (6) (2007) 990–997.
[30] C.P. O'Brien, J.B. Miller, B.D. Morreale, A.J. Gellman, J. Phys. Chem. C 115 (49) (2011) 24221–24230.
[31] B.H. Howard, R.P. Killmeyer, K.S. Rothenberger, A.V. Cugini, B.D. Morreale, R.M. Enick, F. Bustamante, J. Membr. Sci. 241 (2) (2004) 207–218.
[32] E. Kikuchi, Catal. Today 56 (1–3) (2000) 97–101.
[33] I.B. Elkina, J.H. Meldon, Desalination 147 (1–3) (2002) 445–448.
[34] B.D. Morreale, B.H. Howard, O. Iyoha, R.M. Enick, C. Ling, D.S. Sholl, Ind. Eng. Chem. Res. 46 (19) (2007) 6313–6319.
[35] P. Kamakoti, B.D. Morreale, M.V. Ciocco, B.H. Howard, R.P. Killmeyer, A.V. Cugini, D.S. Sholl, Science 307 (5709) (2005) 569–573.
[36] A. Kulprathipanja, G.O. Alptekin, J.L. Falconer, J.D. Way, J. Membr. Sci. 254 (1–2) (2005) 49–62.
[37] S.K. Gade, S.J. DeVoss, K.E. Coulter, S.N. Paglieri, G.O. Alptekin, J.D. Way, J. Membr. Sci. 378 (1–2) (2011) 35–41.
[38] O. Iyoha, R. Enick, R. Killmeyer, B. Howard, M. Ciocco, B. Morreale, J. Membr. Sci. 306 (1–2) (2007) 103–115.
[39] C.G. Sonwane, J. Wilcox, Y.H. Ma, J. Chem. Phys. 125 (18) (2006).
[40] S.K. Gade, E.A. Payzant, H.J. Park, P.M. Thoen, J.D. Way, J. Membr. Sci. 340 (1–2) (2009) 227–233.
[41] K.E. Coulter, J.D. Way, S.K. Gade, S. Chaudhari, D.S. Sholl, L. Semidey-Flecha, J. Phys. Chem. C 114 (40) (2010) 17173–17180.
[42] D.A. McQuarrie, Statistical Mechanics, vol. xii, University Science Books, Sausalito, Calif., 2000. p. 641.